Reactions of Late Lanthanide Metal Atoms with Water Molecules: A Matrix Isolation Infrared Spectroscopic and Theoretical Study

Jia Xu, Xi Jin, and Mingfei Zhou*

Department of Chemistry, Shanghai Key Laboratory of Molecular Catalysts and Innovative Materials, Advanced Materials Laboratory, Fudan University, Shanghai 200433, People's Republic of China

Received: April 19, 2007; In Final Form: May 24, 2007

The reactions of late lanthanide metal atoms (Gd−Lu) with water molecules have been investigated using matrix isolation infrared spectroscopy. The reaction intermediates and products were identified on the basis of isotopic substitution experiments and density functional theory calculations. All of the metal atoms except Lu react with water to form the $M(H_2O)$ complexes spontaneously upon annealing (M = Gd, Tb, Dy, Ho, Er, Tm, and Yb). The $Dy(H_2O)$ and $Ho(H_2O)$ complexes are able to coordinate a second water molecule to form the $Dy(H_2O)_2$ and $Ho(H_2O)_2$ complexes. The $M(H_2O)$ complexes isomerize to the inserted HMOH isomers under visible light irradiation, which further decompose to give the MO and/or HMO molecules upon UV light irradiation. The $M(OH)_2$ molecules (M = Gd−Lu) were also produced. The results have been compared with our earlier work covering the early lanthanide metal atoms (Nd, Sm, Eu) to observe the existent trends for the lanthanide metal atom reactions.

Introduction

With the results reported here, we complete the study on the reactivity of lanthanide metal atoms with water. As has been pointed out in our previous paper regarding the reactions of early lanthanide metal atoms,[1] the reactivity of transition-metal atoms and ions with water has been the subject of considerable experimental and theoretical studies.[2−15] It was found that early transition-metal atoms and ions reacted with water to form the metal monoxide neutrals and cations in the gas phase.[2−8] Matrix isolation infrared spectroscopic studies showed that early transition-metal atoms reacted with water molecules to initially form the HMOH insertion intermediates spontaneously upon annealing.[9−11] The insertion molecules could either photochemically isomerize to the high valent H_2MO isomers or decompose to the metal monoxide and H_2.[9−11] The later transition-metal atoms reacted with water to give primarily the $M(H_2O)$ complexes, which rearranged to the insertion products under UV−visible light excitation.[12,13] Similar investigations on the reactions of f element atoms indicate that actinide metal atoms are more reactive than the transition-metal atoms. It was found that the ground-state thorium and uranium atoms are able to directly insert into the O−H bond of water to form the H_2ThO and H_2UO molecules in low-temperature noble gas matrices.[14,15] Recent investigations in this group found that the early lanthanide metal atoms with a contracted 4f valence shell react with water to form the $M(H_2O)$ and $M(H_2O)_2$ complexes. The $M(H_2O)$ complexes isomerize to the inserted HMOH isomers, and the $M(H_2O)_2$ complexes either decompose to form the trivalent $HNd(OH)_2$ molecule or rearrange to the divalent $Sm(OH)_2$ and $Eu(OH)_2$ molecules under red light irradiation.[1]

In this paper, we present a combined matrix isolation infrared spectroscopic and theoretical study on the reactions of later lanthanide metal atoms (Gd−Lu) with water. The reaction intermediates and products were trapped and identified, and the results are compared with our earlier work covering the early lanthanide metal atoms (Nd, Sm, Eu) to observe the existent trends for the lanthanide metal atom reactions.

Experimental and Theoretical Methods

The experiments for pulsed laser evaporation and matrix isolation infrared spectroscopic investigation are similar to those used previously.[16] Briefly, a Nd:YAG laser fundamental (1064 nm, 10 Hz repetition rate with 10 ns pulse width) was focused onto the rotating metal targets. The laser-evaporated metal atoms were co-deposited with water in excess argon onto a CsI window cooled normally to 6 K by means of a closed-cycle helium refrigerator (ARS, 202N). The matrix gas deposition rate was typically 4 mmol/h. The H_2O/Ar mixtures were prepared in a stainless steel vacuum line using a standard manometric technique. Distilled water was cooled to 77 K using liquid N_2 and evacuated to remove volatile impurities. Isotopically labeled D_2O and $H_2{}^{18}O$ (Cambridge Isotopic Laboratories) were used without further purification. Isotopic exchange with water adsorbed on the walls of the vacuum line occurred readily; in the experiments with the D_2O sample, the HDO and H_2O absorptions were also presented. After sample deposition, IR spectra were recorded on a Bruker IFS66V spectrometer at 0.5 cm^{-1} resolution using a liquid-nitrogen-cooled HgCdTe (MCT) detector for the spectral range of 4000−450 cm^{-1}. Samples were annealed at different temperatures and subjected to broad-band irradiation using a tungsten lamp or a high-pressure mercury arc lamp with glass filters.

Quantum chemical calculations were performed to determine the molecular structures and to help the assignment of vibrational frequencies of the observed reaction products. The calculations were performed at the level of density functional theory (DFT) with the B3LYP method, where the Becke's three parameter hybrid functional and the Lee−Yang−Parr correlation functional were used.[17] The 6-311++G** basis sets were used for the H and O atoms, and the scalar relativistic SDD pseudopotential and basis sets were used for the metal atoms.[18,19] A neutral atom

* To whom correspondence should be addressed. E-mail: mfzhou@fudan.edu.cn.

10.1021/jp073047g CCC: $37.00
Published on Web 07/04/2007

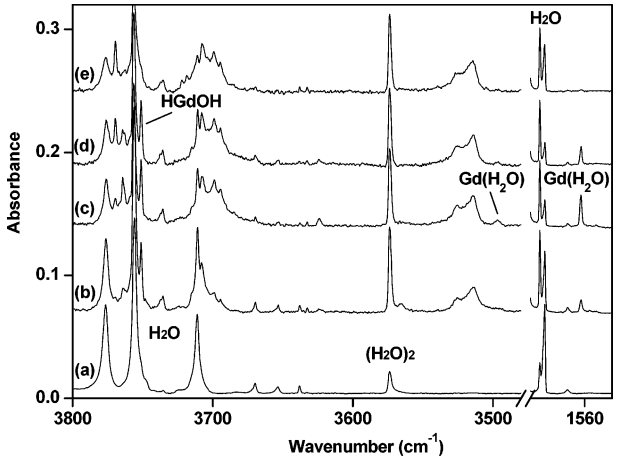

Figure 1. Infrared spectra in the 3800−3480 and 1600−1540 cm^{-1} regions from co-deposition of laser-evaporated Gd atoms with 0.2% H_2O in argon; (a) 1 h of sample deposition at 6 K, (b) after 25 K annealing, (c) after 35 K annealing, (d) after 15 min of $\lambda > 500$ nm irradiation, and (e) after 15 min of $250 < \lambda < 580$ nm irradiation.

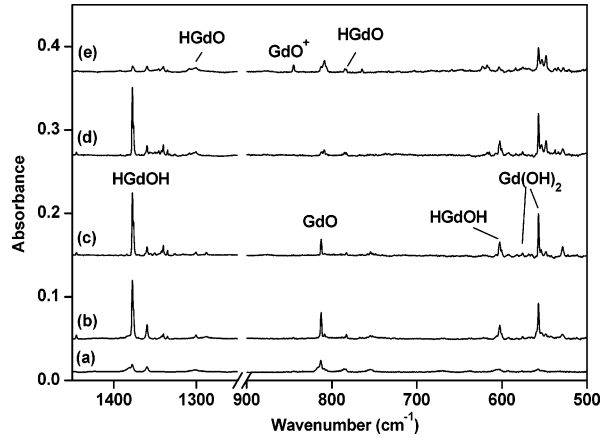

Figure 2. Infrared spectra in the 1450−1300 and 900−500 cm^{-1} regions from co-deposition of laser-evaporated Gd atoms with 0.2% H_2O in argon; (a) 1 h of sample deposition at 6 K, (b) after 25 K annealing, (c) after 35 K annealing, (d) after 15 min of $\lambda > 500$ nm irradiation, and (e) after 15 min of $250 < \lambda < 580$ nm irradiation.

was used as the reference system to generate the pseudopotential and to specify the theoretical level of Wood Boring quasirelativistic. The number of core electrons which were replaced by the pseudopotential was 28 for the Ho, Er, Tm, Yb, and Lu atoms, and part of the f electrons of Gd, Tb, and Dy atoms were also treated as the core electrons.[20] Geometries were fully optimized, and vibrational frequencies were calculated with analytical second derivatives. The single point energies of selected structures optimized at the B3LYP level were calculated using the CCSD(T) method with the same basis sets. These calculations were performed using the Gaussian 03 program.[21]

Results and Discussion

Infrared Spectra. A series of experiments have been performed using different H_2O concentrations (ranging from 0.05 to 0.2% in argon) with different metal targets. The representative infrared spectra in selected regions using the Gd, Ho, and Tm metal targets with 0.2% H_2O in argon are illustrated in Figures 1−5. The spectra with the other metals are shown as Supporting Information. Taking the Gd reaction as an example, weak absorption due to GdO was observed after sample deposition,[22] and new product absorptions were produced upon sample annealing and broad-band irradiation. These new

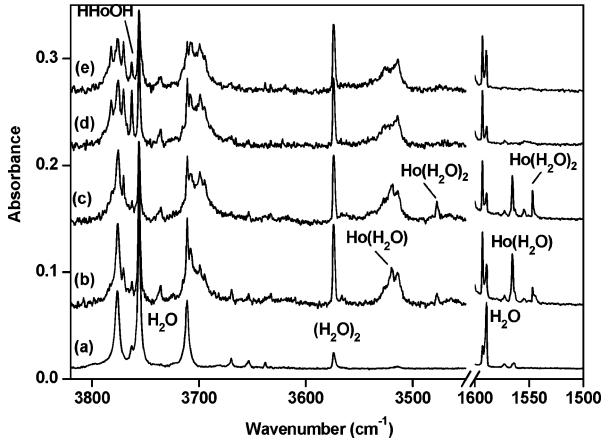

Figure 3. Infrared spectra in the 3820−3450 and 1600−1500 cm^{-1} regions from co-deposition of laser-evaporated Ho atoms with 0.2% H_2O in argon; (a) 1 h of sample deposition at 6 K, (b) after 30 K annealing, (c) after 35 K annealing, (d) after 15 min of $\lambda > 500$ nm irradiation, and (e) after 15 min of $250 < \lambda < 580$ nm irradiation.

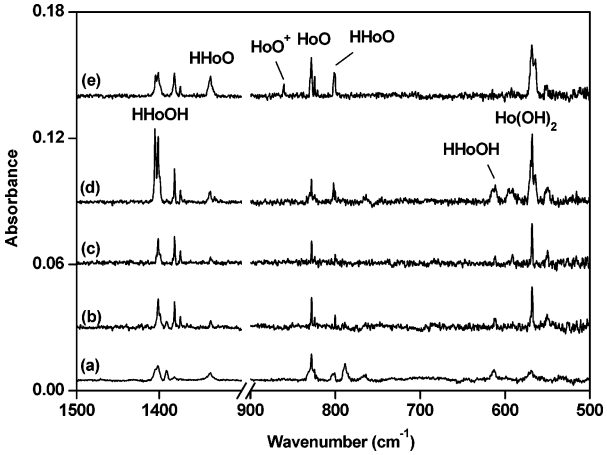

Figure 4. Infrared spectra in the 1500−1300 and 900−500 cm^{-1} regions from co-deposition of laser-evaporated Ho atoms with 0.2% H_2O in argon; (a) 1 h of sample deposition at 6 K, (b) after 30 K annealing, (c) after 35 K annealing, (d) after 15 min of $\lambda > 500$ nm irradiation, and (e) after 15 min of $250 < \lambda < 580$ nm irradiation.

absorptions can be classified into several groups based on their annealing and photochemical behaviors. The 3496.1 and 1562.7 cm^{-1} absorptions appeared upon sample annealing to 25 K (Figure 1, trace b), markedly increased upon sample annealing to 35 K (Figure 1, trace c), but decreased when the matrix sample was irradiated by the output of a tungsten lamp with a 500 nm long-wavelength pass filter and disappeared upon continued broad-band irradiation with the high-pressure mercury arc lamp ($250 < \lambda < 580$ nm). The 3751.2, 1377.4, and 602.4 cm^{-1} absorptions were weak upon sample deposition, increased upon sample annealing, remained almost unchanged upon $\lambda > 500$ nm irradiation, but almost disappeared upon $250 < \lambda < 580$ nm broad-band irradiation. The 3764.3, 575.7, and 556.9 cm^{-1} absorptions were produced upon sample annealing to 25 K, increased upon sample annealing to high temperatures, but decreased upon $250 < \lambda < 580$ nm irradiation, during which the GdO and GdO^+ absorptions were produced.[22] Weak absorptions at 1300.6 and 782.7 cm^{-1} also increased upon broad-band irradiation, as illustrated in Figure 2.

The band positions of the observed product absorptions are listed in Tables 1−5. Experiments were repeated by using the isotopically labeled $H_2{}^{18}O$, D_2O, and $H_2{}^{16}O + H_2{}^{18}O$ mixtures for selected metals. Figure 6 shows the spectra in the 850−500 cm^{-1} region from co-deposition of laser-evaporated Gd atoms

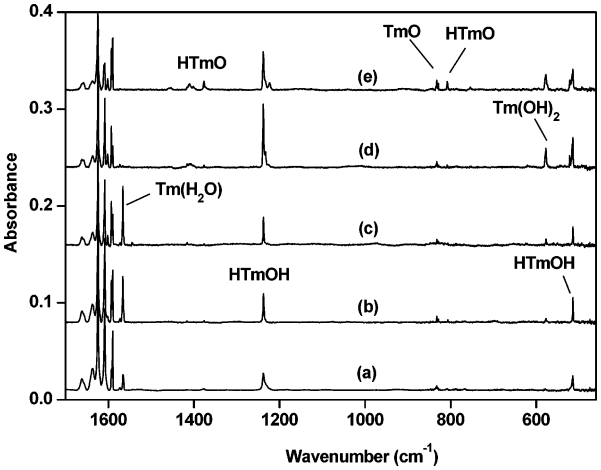

Figure 5. Infrared spectra in the 1700−460 cm^{-1} region from co-deposition of laser-evaporated Tm atoms with 0.2% H_2O in argon; (a) 1 h of sample deposition at 6 K, (b) after 20 K annealing, (c) after 30 K annealing, (d) after 15 min of $\lambda > 500$ nm irradiation, and (e) after 15 min of $250 < \lambda < 580$ nm irradiation

TABLE 1: Observed and Calculated Vibrational Frequencies (cm^{-1}) of the M(H_2O) Complexes (M = Gd−Yb)

	sym H_2O stretch		H_2O bending	
molecule	obsd	calcd	obsd	calcd
Gd(H_2O)	3496.1	3582.3	1562.7	1571.6
Tb(H_2O)	3480.6	3643.6	1559.4	1585.1
Dy(H_2O)	3514.7	3645.3	1563.7	1584.6
Ho(H_2O)	3519.2	3639.2	1565.4	1583.7
Er(H_2O)		3643.2	1565.1	1586.9
Tm(H_2O)	3522.1	3638.1	1565.7	1583.7
Yb(H_2O)	3531.3	3641.9	1568.9	1586.5

TABLE 2: Observed and Calculated Vibrational Frequencies (cm^{-1}) of the Dy(H_2O)$_2$ and Ho(H_2O)$_2$ Complexes

	HOH stretch		asym H_2O bending	
molecule	obsd	calcd	obsd	calcd
Dy(H_2O)$_2$	3473.6	3643.2	1545.9	1578.1
Ho(H_2O)$_2$	3477.9	3624.5	1546.9	1574.7
Ho($H_2{}^{18}O$)$_2$	3471.6	3616.8	1540.2	1567.4
Ho(D_2O)$_2$		2611.4	1147.4	1154.4

TABLE 3: Observed and Calculated Vibrational Frequencies (cm^{-1}) of the HMOH Molecules (M = Gd−Lu)

	OH stretch		M−H stretch		M−OH stretch	
molecule	obsd	calcd	obsd	calcd	obsd	calcd
HGdOH	3751.2	3967.5	1377.4	1399.8	602.4	597.5
HTbOH	3755.8	3970.9	1388.0	1406.6	609.3	600.0
HDyOH		3973.0	1390.7	1410.0	619.3	602.3
HHoOH	3762.7	3960.9	1401.3	1399.3	611.6	624.5
HErOH	3764.9	3956.6	1409.9	1411.6	623.4	627.3
HTmOH		3951.8	1237.1	1249.7	514.0	540.1
HYbOH	3756.0	3954.4	1238.6	1263.2	511.8	530.2
HLuOH		3967.4	1423.1	1455.5	629.0	636.3

with the H_2O, $H_2{}^{16}O + H_2{}^{18}O$, and $H_2O + D_2O$ samples, while Figure 7 shows the infrared spectra in the 1640−1530 and 860−500 cm^{-1} regions from co-deposition of laser-evaporated Ho atoms with a 0.1% $H_2{}^{16}O$ + 0.1% $H_2{}^{18}O$ mixtures. The isotopic counterparts are provided in Supporting Information. The reaction products are assigned on the basis of the isotopic shifts and splittings of the observed product absorptions as well as DFT frequency calculations.

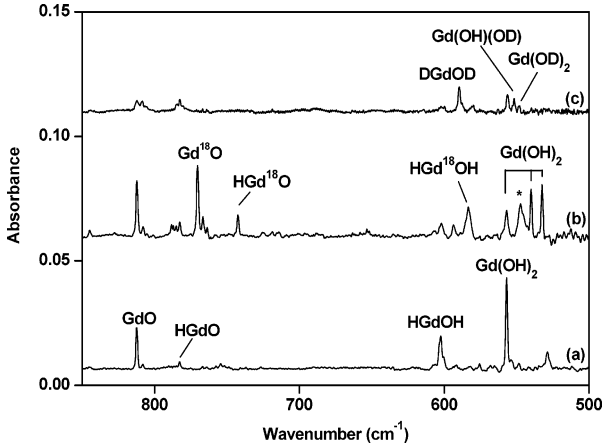

Figure 6. Infrared spectra in the 850−500 cm^{-1} region from co-deposition of laser-evaporated Gd atoms with isotopic labeled samples. Spectra were taken after 1 h of sample deposition followed by 25 K annealing; (a) 0.2% H_2O, (b) 0.1% $H_2{}^{16}O$ + 0.1% $H_2{}^{18}O$, and (c) 0.1% H_2O + 0.1% D_2O (the asterisk denotes an impurity absorption).

TABLE 4: The Calculated Geometric Parameters (Bond Lengths in Angstroms, Bond Angles in Degrees) and the Observed and Calculated Vibrational Frequencies (cm^{-1}) of the HMO Molecules (M = Gd−Tm)

	geometric parameters			M−H stretch		M−O stretch	
molecule	M−H	M−O	∠HMO	obsd	calcd	obsd	calcd
HGdO (^{8}A′)	2.063	1.882	107.3	1300.6	1346.4	782.7	785.4
HTbO (^{7}A″)	2.031	1.797	111.6	1310.1	1349.4	793.4	846.6
HDyO (^{6}A″)	2.035	1.861	107.8	1316.1	1370.1	798.2	790.6
HHoO (^{5}A′)	2.022	1.805	112.6	1337.6	1392.1	800.2	836.8
HErO (^{4}A″)	2.002	1.804	112.1	1363.2	1402.7	801.3	837.4
HTmO (^{3}A′)	2.004	1.800	114.5	1376.3	1363.3	806.4	820.3

TABLE 5: Observed and Calculated Vibrational Frequencies (cm^{-1}) of the M($OH)_2$ Molecules (M = Gd−Yb)

	asym OH stretch		sym MOH stretch		asym MOH stretch	
molecule	obsd	calcd	obsd	calcd	obsd	calcd
Gd($OH)_2$	3764.3	3967.5	575.7	592.2	556.9	562.2
Tb($OH)_2$	3764.7	3968.9	582.9	594.8	563.8	564.8
Dy($OH)_2$	3769.4	3971.3		596.9		566.5
Ho($OH)_2$	3770.6	3952.3		611.5	568.0	577.6
Er($OH)_2$	3772.2	3953.6		618.3	572.1	584.9
Tm($OH)_2$	3769.8	3966.1		621.0	576.9	588.4
Yb($OH)_2$	3766.8	3960.1	503.4	523.6	490.6	515.6

M(H_2O). Reactions of Gd, Tb, Dy, Ho, Er, Tm, and Yb atoms with water molecules revealed quite strong absorptions in the 1560−1570 cm^{-1} region (Gd, 1562.7; Tb, 1559.4; Dy, 1563.7; Ho, 1565.4; Er, 1565.1; Tm, 1565.7; Yb, 1568.9 cm^{-1}). These absorptions were produced upon sample annealing and were destroyed upon broad-band irradiation. In the O−H stretch frequency region, absorptions at 3496.1, 3480.6, 3514.7, 3519.2, 3522.1, and 3531.3 cm^{-1} for Gd, Tb, Dy, Ho, Tm, and Yb tracked with the absorptions around 1565 cm^{-1}. These absorptions are assigned to the M(H_2O) complexes. Taking the Ho + H_2O reaction as an example, the 1565.4 cm^{-1} absorption shifted to 1558.9 and 1160.0 cm^{-1}, respectively, with the $H_2{}^{18}O$ and D_2O samples. The band position and isotopic $^{16}O/^{18}O$ and H/D ratios indicate that this absorption is due to the H_2O bending vibration of a metal−water complex. The experiment with 1:1 mixtures of $H_2{}^{16}O$ and $H_2{}^{18}O$ (Figure 7) implies that only one H_2O subunit is involved in this mode. The 3519.2 cm^{-1} absorption is much weaker than the 1565.4 cm^{-1} absorption and is due to the symmetric OH stretch mode of the Ho(H_2O)

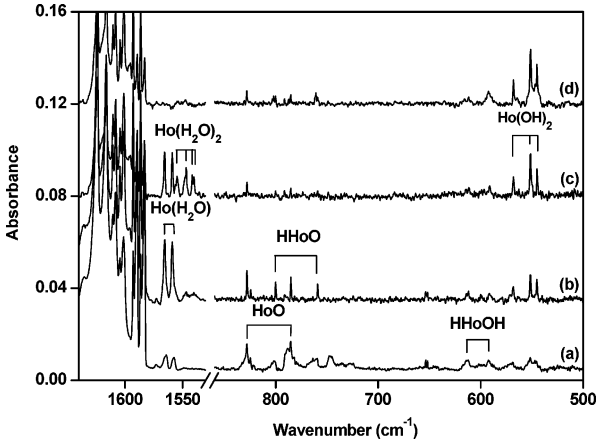

Figure 7. Infrared spectra in the 1640−1530 and 860−500 cm^{-1} regions from co-deposition of laser-evaporated Ho atoms with 0.1% $H_2{}^{16}O$ + 0.1% $H_2{}^{18}O$ in argon; (a) 1 h of sample deposition at 6 K, (b) after annealing to 25 K, (c) after annealing to 30 K, and (d) after 15 min of 250 < λ < 580 nm irradiation.

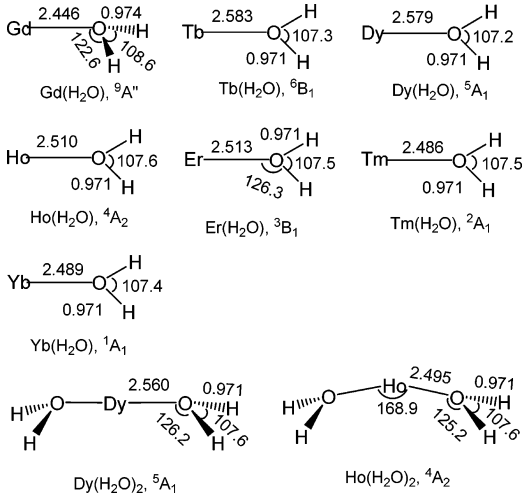

Figure 8. Optimized structures of the $M(H_2O)$ and $M(H_2O)_2$ complexes (bond lengths in angstroms, bond angles in degrees).

complex. The $Lu(H_2O)$ complex was not observed in the experiments.

The assignments are supported by DFT calculations. As shown in Figure 8, the $Gd(H_2O)$ complex was predicted to have a $^9A''$ ground state with a nonplanar C_s symmetry, whereas the other $M(H_2O)$ (M = Tb, Dy, Ho, Er, Tm, and Yb) complexes were predicted to have planar structures with C_{2v} symmetry. The electron configurations of ground-state $M(H_2O)$ complexes (Gd, $^9A''$; Tb, $^6B_1$; Dy, $^5A_1$; Ho, $^4A_2$; Er, $^3B_1$; Tm, $^2A_1$; Yb, $^1A_1$) correlate to the ground state of the metal atoms. The calculated vibrational frequencies for the $M(H_2O)$ complexes are compared with the experimental values in Table 1. The H_2O bending and symmetric HOH stretch modes were predicted to have appreciable IR intensities, which were experimentally detected with their frequencies and isotopic frequency shifts in good agreement with the experimental values. The antisymmetric HOH stretch modes of the $M(H_2O)$ complexes were predicted to be about 100 cm^{-1} higher than the symmetric stretch modes but with very low IR intensities, and thus, they were not observed in the experiments.

$M(H_2O)_2$ (M = Dy, Ho) In the Dy and Ho systems, new absorptions in the H_2O bending and O−H stretch frequency regions were observed besides the $M(H_2O)$ absorptions. These absorptions were produced upon annealing after the $M(H_2O)$ absorptions (Figure 3) and are favored relative the $M(H_2O)$ absorptions with high H_2O concentrations. This experimental observation implies that the absorber involves more than one H_2O subunit. In the experiment of Ho with equal molecular mixtures of $H_2{}^{16}O$ and $H_2{}^{18}O$, four absorptions positioned at 1554.8, 1546.9, 1541.6, and 1540.2 cm^{-1} were clearly resolved for the low-frequency mode (Figure 7). This spectral feature indicates that the complex involves two equivalent H_2O subunits and, therefore, are assigned to the $Ho(H_2O)_2$ complex. The 1546.9 cm^{-1} absorption is due to the antisymmetric bending mode; the symmetric bending mode of $Ho(H_2{}^{16}O)_2$ and $Ho(H_2{}^{18}O)_2$ was not observed, but this mode for the $Ho(H_2{}^{16}O)(H_2{}^{18}O)$ isotopomer was observed at 1554.8 cm^{-1}. The $Nd(H_2O)_2$, $Sm(H_2O)_2$, and $Eu(H_2O)_2$ complexes have been observed in our earlier study.[1]

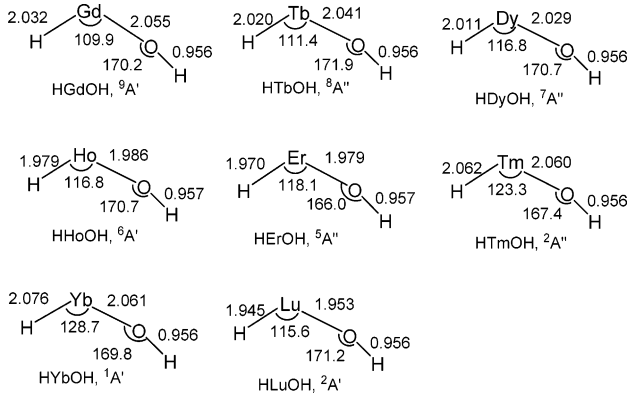

Figure 9. Optimized structures of the inserted HMOH molecules (M = Gd−Lu, bond lengths in angstroms, bond angles in degrees).

The $Dy(H_2O)_2$ and $Ho(H_2O)_2$ complexes were calculated to have an $^5A_1$ and $^4A_2$ ground state with C_{2v} symmetry (Figure 8), which correlates with the $f^{10}d^0s^2$ and $f^{11}d^0s^2$ ground state of the metal atoms. The calculated H_2O bending and O−H stretch vibrational frequencies of the $Dy(H_2O)_2$ and $Ho(H_2O)_2$ complexes were compared with the observed values in Table 2. No evidence was found for the formation of the $Gd(H_2O)_2$, $Tb(H_2O)_2$, $Er(H_2O)_2$, $Tm(H_2O)_2$, and $Yb(H_2O)_2$ complexes in the present experiments.

HMOH. For all of the metal systems studied here, new product absorptions were observed in the O−H, M−H, and M−O stretch frequency regions, as listed in Table 3. These absorptions are assigned to the inserted HMOH molecules. The HMOH molecules were predicted to have planar structures with C_s symmetry (Figure 9). The ∠HMO ranges from 109.9° in HGdOH to 128.7° in HYbOH. As listed in Table 3, the calculated O−H, M−H, and M−O stretch frequencies match the experimental values and support the experimental assignments.

The HGdOH molecule was predicted to have an $^9A'$ ground state with a Gd f^7s^1 electron subconfiguration. The HTmOH, HYbOH, and HLuOH molecules have $^2A''$,$^1A'$, and $^2A'$ ground states. Surprisingly, the HTbOH, HDyOH, HHoOH, and HErOH molecules were determined to have $^8A''$, $^7A''$, $^6A'$, and $^5A''$ ground states, respectively, with the metals in $f^{n-1}s^1$ subconfigurations. Taking the HHoOH as an example, the $^4A''$ state with a Ho f^{11} subconfiguration was predicted to be 3.2 kcal/mol lower in energy than the $^6A'$ state with a Ho $f^{10}s^1$ subconfiguration at the B3LYP level. However, the $^6A'$ state is more stable than the $^4A''$ state at the CCSD(T) level of theory. The Ho−H and Ho−OH stretch frequencies for the $^6A'$ state HHoOH were calculated at 1399.3 and 624.5 cm^{-1}, which fit the experimental values very well. The Ho−H and Ho−OH stretch modes of the $^4A''$ state were calculated to be 1240.3

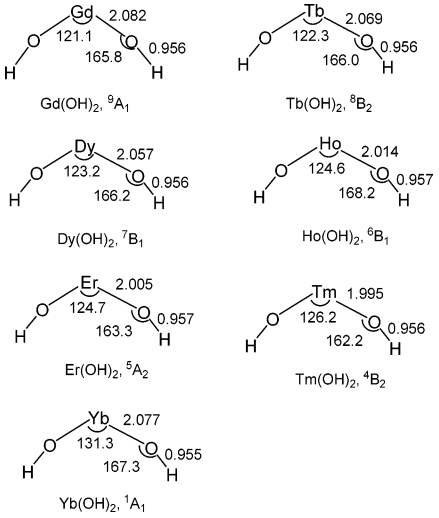

Figure 10. Optimized structures of the $M(OH)_2$ molecules (M = Gd−Yb, bond lengths in angstroms, bond angles in degrees).

and 526.3 cm^{-1}, too low to fit the experimental values. A similar situation exists for the HTbOH, HDyOH, and HErOH molecules.

HMO. Absorptions at 1300.6 and 782.7 cm^{-1} for Gd, 1310.1 and 793.4 cm^{-1} for Tb, 1316.1 and 798.2 cm^{-1} for Dy, 1337.6 and 800.2 cm^{-1} for Ho, 1363.2 and 801.3 cm^{-1} for Er, and 1376.3 and 806.4 cm^{-1} for Tm were produced mainly upon broad-band irradiation (Figures 2, 4, and 5). The isotopic substitution experiments indicate that the upper mode is due to a M−H stretch vibration, while the low mode is a terminal M−O stretch mode. These absorptions are assigned to the M−H and M−O stretch modes of the HMO molecules (Table 4). The HMO molecules were predicted to have bent structures with $^8A'$, $^7A''$, $^6A''$, $^5A'$, $^4A''$, and $^3A'$ ground states for Gd, Tb, Dy, Ho, Er, and Tm, respectively. The Lewis structure of the HMO molecule can be drawn as H−M═O, with the metal in the formal +3 oxidation state. No absorptions were observed in the Yb + H_2O experiments that can be assigned to the analogous HYbO molecule. Yb is an atypical lanthanide with a completely filled 4f shell ($4f^{14}5d^06s^2$) and exhibits a formal oxidation state of +2.

$M(OH)_2$. Besides the above-characterized product absorptions, new absorptions were observed in the M−OH stretch frequency region for all of the metal systems studied here except Dy and Lu; see Table 5. All of these absorptions increased upon sample annealing and/or broad-band irradiation using a 500 nm long-wavelength pass filter with a tungsten lamp. The band positions and isotopic shifts indicate that these absorptions are due to M−OH stretch vibrations. The triplet isotopic structures in the experiments with equal molar mixtures of $H_2{}^{16}O$ and $H_2{}^{18}O$ confirmed the involvement of two equivalent OH subunits (the mixed spectra of the Gd and Ho reaction systems are shown in Figures 6 and 7, respectively). In the O−H stretch frequency region, absorptions at 3764.3 (Gd), 3764.7 (Tb), 3770.6 (Ho), 3772.2 (Er), 3769.8 (Tm), and 3766.8 cm^{-1} (Yb) were tracked with the M−OH stretch frequencies. No absorptions in the M−H stretch frequency region were observed to track with these absorptions. Accordingly, these absorptions are assigned to the $M(OH)_2$ molecules (Table 5).

The optimized structures of the $M(OH)_2$ molecules are shown in Figure 10. All of the $M(OH)_2$ molecules were predicted to be bent with ∠OMO ranges from 121.1 (Gd) to 131.3° (Yb). The $Gd(OH)_2$ molecule was predicted to have an $^9A_1$ ground state with a Gd f^7s^1 subconfiguration. The $M(OH)_2$ molecules with M = Tb, Dy, Ho, Er, and Tm were calculated to have $^8B_2$, $^7B_1$, $^6B_1$, $^5A_2$, and $^4B_2$ ground states, respectively, which correlate to a $4f^{n-1}5d^16s^2$ electron configuration of the metal atoms. The ground state of $Yb(OH)_2$ is $^1A_1$. As listed in Table 5, the calculated antisymmetric O−H and M−OH stretch frequencies are in good agreement with the observed values. The symmetric stretch modes were predicted to have low IR intensities and were not observed.

Reaction Mechanism. The reactions of late lanthanide atoms (Gd−Yb) with water molecules are similar to those early lanthanide metals that we have reported earlier.[1] The initial step is the formation of the $M(H_2O)$ complexes, reaction 1. These association reactions were predicted to be exothermic. The complex absorptions increased upon annealing, suggesting that the reactions require negligible activation energy

$$M + H_2O \rightarrow M(H_2O)\ (M = Gd, Tb, Dy, Ho, Er, Tm, Yb) \quad (1)$$

Similar to the early lanthanide metals Nd, Eu, and Sm, the $Dy(H_2O)$ and $Ho(H_2O)$ complexes can further react with water to form the $Dy(H_2O)_2$ and $Ho(H_2O)_2$ complexes

$$Dy(H_2O)\ (^5A_1) + H_2O\ (^1A_1) \rightarrow Dy(H_2O)_2\ (^5A_1)$$
$$\Delta E = -9.9\ \text{kcal/mol} \quad (2)$$

$$Ho(H_2O)\ (^4A_2) + H_2O\ (^1A_1) \rightarrow Ho(H_2O)_2\ (^4A_2)$$
$$\Delta E = -9.4\ \text{kcal/mol} \quad (3)$$

The $M(H_2O)$ complex absorptions almost disappeared upon $\lambda > 500$ nm irradiation, during which the HMOH absorptions increased. The HMOH molecules were formed by isomerization reactions

$$M(H_2O) \rightarrow HMOH\ (M = Gd, Tb, Dy, Ho, Er, Tm, Yb) \quad (4)$$

All of the isomerization reactions were predicted to be exothermic but require activation energies. The reactions proceeded experimentally under red light irradiation, suggesting that the energy barriers are low. In some reaction systems, the HMOH absorptions also increased upon annealing, which is due to the red irradiation from the IR spectrometer that can induce isomerization. In our earlier study on the early lanthanide metal atom reactions, the energy barriers were calculated to be less than 20 kcal/mol.[1]

For all of the metal systems except Yb, the HMOH absorptions almost disappeared under $250 < \lambda < 580$ nm irradiation, during which the MO and/or HMO absorptions markedly increased. This observation suggests that the HMOH molecules decomposed to form the MO and/or HMO molecules. The HLuOH absorptions were very weak; therefore, no obvious LuO and HLuO absorptions were observed. The HYbOH absorptions remained almost unchanged upon irradiation. As has been mentioned above, Yb is an atypical lanthanide with a formal oxidation state of +2. The HYbO molecule with Yb in its +3 oxidation state is not expected to be formed.

For all of the metal systems except Lu, the $M(OH)_2$ absorptions were also observed. The $Dy(OH)_2$ and $Ho(OH)_2$ molecules were formed largely upon visible light irradiation at the expense of the $Dy(H_2O)_2$ and $Ho(H_2O)_2$ absorptions, whereas the other $M(OH)_2$ absorptions were produced upon sample annealing. These experimental observations suggest that the metal atoms react with two water molecules to form the $M(OH)_2$ molecules via the $M(H_2O)_2$ intermediates. For Gd, Tb, Er, Tm,

and Yb, the $M(H_2O)_2$ intermediates are short-lived species and were not able to be stabilized in the matrix.

So far, we have performed the experiments on the reactions of almost the whole period of lanthanide metal atoms with water molecules except Pr and Pm. The experimental observations indicate that the neutral lanthanide metal atoms are able to coordinate water to form the $M(H_2O)$ and $M(H_2O)_2$ complexes. The coordination of only one and two water molecules for neutral lanthanide metal atoms is quite different with the lanthanide metal cations, which can coordinate up to nine water molecules.[23] One may expect that the rigid matrix as well as the low water concentrations used in the experiments may be an important factor to control the number of water molecules coordinated around the lanthanide atom. However, water aggregates formed readily upon sample annealing with a water concentration of 0.2% in argon, which suggests that the limitation controlling the number of coordinated water molecules is not due to a rigid matrix and low water concentrations. As has been discussed in our previous article,[1] the water ligand is a σ donor but not a π acceptor. When forming a metal−water complex, the move of the water charge to the neutral metal atom results in negative charge accumulation on the metal center, which prevents further water coordination. It is interesting to note that while all of the metal atoms except Lu react with water to form the $M(H_2O)$ complex, only the Nd, Sm, Eu, Dy, and Ho atoms are able to coordinate two water molecules to form the $M(H_2O)_2$ complexes. Two origins for such difference are conceivable, (1) the repulsion between the d electron of the lanthanide atom and the lone pair electrons of the O atom and (2) the number of 4f electrons. Note that the metal atoms Nd, Sm, Eu, and Ho, which are able to coordinate two water molecules, all have a $4f^n5d^06s^2$ electron configuration, whereas the metal atoms which can only coordinate one water molecule have a $4f^{n-1}5d^16s^2$ electron configuration, except Tb, Er, Tm, and Yb. For Tb, the energy gap between the ground state with a $4f^95d^06s^2$ configuration and the first excited state with a $4f^8$-$5d^16s^2$ configuration is very small.[24] We found that when the number of the metal 4f electrons goes beyond 11 (Er−Yb), the metal atoms can only coordinate one water molecule, despite the fact that metal atoms do not have 5d electron population. That is, there is a turning point between the Ho element with 11 f electrons and Er with 12 f electrons. In fact, the existence of the turning point is a common phenomenon in both physical and chemical properties of lanthanide compounds, for example, the famous "tetrad effect".[25] With an increase in the number of 4f electrons, the repulsion between the interelectrons becomes much stronger, which prevents the coordination of more than one water molecules to the metal atom when the number of f electrons reaches 12. Consistent with this notion, we found that the Lu metal atom, which has an electron configuration of $4f^{14}$-$5d^16s$,[2] was not able to form the $Lu(H_2O)$ complex in a solid argon matrix. The behavior of Lu is quite similar to that of the group IIIB metals with an $(n-1)d^1ns^2$ valence electron configuration.[10]

For all of the lanthanide metal systems studied, the inserted HMOH molecules were experimentally observed. The bonding behavior among the HMOH molecules is quite appealing. A plot of all of the presently available M−H stretch frequencies of HMOH is shown in Figure 11. A "double-concave" graph is obtained. We can roughly draw two lines based on the points shown in Figure 11; one involves the Ce, Gd, Tb, Dy, Ho, Er, and Lu series, and another one involves the Nd, Sm, Eu, Tm, and Yb series. These two lines are almost parallel, with a gap of about 200 cm^{-1}. The M−H stretch frequencies increase along

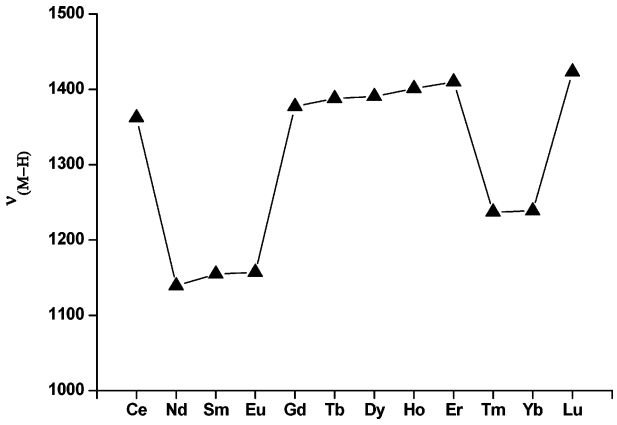

Figure 11. Plot of the M−H stretch frequencies (cm^{-1}) in the HMOH molecules (M = lanthanide metals).

the series, mainly owing to lanthanide contraction. According to the theoretical calculations, all of the metals in the ground state of HMOH have f^ns^1 subconfigurations in the upper series, whereas the metals in the ground state of HMOH have f^n subconfigurations in the low series. The Ce, Gd, and Lu atoms possess a $4f^n5d^16s^2$ ($n = 1, 7, 14$) ground-state configuration. The elements Tb, Dy, Ho, and Er have a $4f^n5d^06s^2$ ground-state configuration, but these elements have a very low-lying $4f^{n-1}5d^16s^2$ excited state,[24] which is much more favorable for bonding. The Nd, Sm, Eu, Tm, and Yb metals in the low series possess a $4f^n5d^06s^2$ ground-state configuration. For Sm and Eu, the first excited state has a $4f^n5d^16s^1$ configuration instead of $4f^{n-1}5d^16s^2$; for Tm, the first excited state has a $4f^{n-1}5d^16s^2$ configuration, but the $4f^n5d^06s^2$ to $4f^{n-1}5d^16s^2$ promotion energy is much higher than that for Tb, Dy, Ho, and Er.[24] Yb has the first excited state of $4f^n6s^16p^1$ structure, which is energetically much higher than the $4f^n5d^06s^2$ ground state. Surprisingly, there is also a small energy gap for Nd between the first excited state with a $4f^{n-1}5d^16s^2$ configuration and the ground state with a $4f^n5d^06s^2$ configuration, which is the main reason to form the relatively stable trivalent $HNd(OH)_2$ molecule, as interpreted in our previous article. However, we found that Nd has a f^ns^0 subconfiguration in HNdOH.

Conclusions

The reactions of late lanthanide metal atoms with water have been studied using the matrix isolation infrared absorption spectroscopy. All of the metal atoms except Lu react with water to form the $M(H_2O)$ complexes, which isomerize to the inserted HMOH isomers under red light irradiation. The HMOH molecules further decompose to form the MO and/or HMO molecules upon UV light irradiation. The $M(OH)_2$ molecules are also formed via the $M(H_2O)_2$ intermediates, which were observed for $Dy(H_2O)_2$ and $Ho(H_2O)_2$. The results have been compared with our earlier work covering the reactions of early lanthanide metals Nd, Sm, and Eu, and several existent trends can be drawn.

(1) Similar to the transition-metal atom reactions, the $M(H_2O)$ complexes and the inserted HMOH molecules are important intermediates in the reactions between lanthanide metal atoms and water.

(2) While all of the metal atoms except Lu react with water to form the $M(H_2O)$ complex, only the Nd, Sm, Eu, Dy, and Ho atoms are able to coordinate two water molecules to form the $M(H_2O)_2$ complexes.

(3) For all of the lanthanide metal systems studied, the inserted HMOH molecules were experimentally observed. These

inserted molecules can be classified into two series. One series involves Ce, Gd, Tb, Dy, Ho, Er, and Lu, which exhibit higher M−H stretch frequencies than those of another series, which includes Nd, Sm, Eu, Tm, and Yb. The first series of HMOH molecules has high-spin ground states with a $f^n s^1$ subconfiguration of the metals, while the second series of HMOH molecules has low-spin ground states with a f^n subconfiguration of the metals.

(4) The different bonding behavior in the lanthanide series is a direct consequence of the change in valence electron configuration of the metals.

Acknowledgment. This work is supported by NKBRSF (2004CB719501) and NNSFC (20433080).

Supporting Information Available: Tables listing the observed and calculated isotopic vibrational frequencies of the $M(H_2O)$, HMOH, HMO, and $M(OH)_2$ (M = Gd, Ho, Er, and Yb) molecules and the infrared spectra of the Tb, Dy, Er, and Yb reactions. This material is available free of charge via the Internet at http://pubs.acs.org.

References and Notes

(1) Xu, J.; Zhou, M. F. *J. Phys. Chem. A* **2006**, *110*, 10575.

(2) Liu, K.; Parson, J. M. *J. Chem. Phys*. **1978**, *68*, 1794.

(3) Tilson, J. L.; Harrison, J. F. *J. Phys. Chem*. **1991**, *95*, 5097.

(4) Guo, B. C.; Kerns, K. P.; Castleman, A. W. *J. Phys. Chem*. **1992**, *96*, 4879.

(5) (a) Clemmer, D. E.; Aristov, N.; Armentrout, P. B. *J. Phys. Chem*. **1994**, *98*, 6522. (b) Chen, Y. M.; Clemmer, D. E.; Armentrout, P. B. *J. Phys. Chem*. **1994**, *98*, 11490.

(6) (a) Irigoras, A.; Fowler, J. E.; Ugalde, J. M. *J. Phys. Chem. A* **1998**, *102*, 293. (b) Irigoras, A.; Fowler, J. E.; Ugalde, J. M. *J. Am. Chem. Soc*. **1999**, *121*, 574. (c) Irigoras, A.; Fowler, J. E.; Ugalde, J. M. *J. Am. Chem. Soc*. **1999**, *121*, 8549. (d) Irigoras, A.; Fowler, J. E.; Ugalde, J. M. *J. Am. Chem. Soc*. **2000**, *122*, 114.

(7) (a) Rosi, M.; Bauschlicher, C. W., Jr. *J. Chem. Phys.* **1989**, *90*, 7264. (b) Rosi, M.; Bauschlicher, C. W., Jr. *J. Chem. Phys*. **1990**, *92*, 1876. (c) Siegbahn, P. E. M.; Blomberg, M. R. A.; Svensson, M. *J. Phys. Chem*. **1993**, *97*, 2564.

(8) (a) Guo, J. Z.; Goodings, J. M. *Chem. Phys. Lett.* **2001**, *342*, 169. (b) Hwang, D. Y.; Mebel, A. M. *Chem. Phys. Lett.* **2001**, *341*, 393.

(9) Kauffman, J. W.; Hauge, R. H.; Margrave, J. L. *J. Phys. Chem.* **1985**, *89*, 3541.

(10) (a) Zhang, L. N.; Dong, J.; Zhou, M. F. *J. Phys. Chem. A* **2000**, *104*, 8882. (b) Zhang, L. N.; Shao, L. M.; Zhou, M. F. *Chem. Phys.* **2001**, *272*, 27.

(11) (a) Zhou, M. F.; Zhang, L. N.; Dong, J.; Qin, Q. Z. *J. Am. Chem. Soc.* **2000**, *122*, 10680. (b) Zhou, M. F.; Dong, J.; Zhang, L. N.; Qin, Q. Z. *J. Am. Chem. Soc*. **2001**, *123*, 135.

(12) Kauffman, J. W.; Hauge, R. H.; Margrave, J. L. *J. Phys. Chem.* **1985**, *89*, 3547.

(13) (a) Zhou, M. F.; Zhang, L. N.; Shao, L. M.; Wang, W. N.; Fan, K. N.; Qin, Q. Z. *J. Phys. Chem. A* **2001**, *105*, 5801. (b) Zhang, L. N.; Zhou, M. F.; Shao, L. M.; Wang, W. N.; Fan, K. N.; Qin, Q. Z. *J. Phys. Chem. A* **2001**, *105*, 6998.

(14) Liang, B. Y.; Andrews, L.; Li, J.; Bursten, B. E. *J. Am. Chem. Soc.* **2002**, *124*, 6723.

(15) Liang, B. Y.; Hunt, R. D.; Kushto, G. P.; Andrews, L.; Li, J.; Bursten, B. E. *Inorg. Chem.* **2005**, *44*, 2159.

(16) (a) Zhou, M. F.; Andrews, L.; Bauschlicher, C. W., Jr. *Chem. Rev.* **2001**, *101*, 1931. (b) Wang, G. J.; Gong, Y.; Chen, M. H.; Zhou, M. F. *J. Am. Chem. Soc*. **2006**, *128*, 5974.

(17) (a) Becke, A. D. *J. Chem. Phys*. **1993**, *98*, 5648. (b) Lee, C.; Yang, W.; Parr, R. G. *Phys. Rev. B* **1988**, *37*, 785.

(18) (a) McLean, A. D.; Chandler, G. S. *J. Chem. Phys*. **1980**, *72*, 5639. (b) Krishnan, R.; Binkley, J. S.; Seeger, R.; Pople, J. A. *J. Chem. Phys*. **1980**, *72*, 650.

(19) Dolg, M.; Stoll, H.; Preuss, H. *J. Chem. Phys.* **1989**, *90*, 1730.

(20) Strange, P.; Svane, A.; Temmerman, W. M.; Szotek, Z.; Winter, H. *Nature* **1999**, *399*, 756.

(21) Frisch, M. J.; Trucks, G. W.; Schlegel, H. B.; Scuseria, G. E.; Robb, M. A.; Cheeseman, J. R.; Montgomery, J. A., Jr.; Vreven, T.; Kudin, K. N.; Burant, J. C.; Millam, J. M.; Iyengar, S. S.; Tomasi, J.; Barone, V.; Mennucci, B.; Cossi, M.; Scalmani, G.; Rega, N.; Petersson, G. A.; Nakatsuji, H.; Hada, M.; Ehara, M.; Toyota, K.; Fukuda, R.; Hasegawa, J.; Ishida, M.; Nakajima, T.; Honda, Y.; Kitao, O.; Nakai, H.; Klene, M.; Li, X.; Knox, J. E.; Hratchian, H. P.; Cross, J. B.; Bakken, V.; Adamo, C.; Jaramillo, J.; Gomperts, R.; Stratmann, R. E.; Yazyev, O.; Austin, A. J.; Cammi, R.; Pomelli, C.; Ochterski, J. W.; Ayala, P. Y.; Morokuma, K.; Voth, G. A.; Salvador, P.; Dannenberg, J. J.; Zakrzewski, V. G.; Dapprich, S.; Daniels, A. D.; Strain, M. C.; Farkas, O.; Malick, D. K.; Rabuck, A. D.; Raghavachari, K.; Foresman, J. B.; Ortiz, J. V.; Cui, Q.; Baboul, A. G.; Clifford, S.; Cioslowski, J.; Stefanov, B. B.; Liu, G.; Liashenko, A.; Piskorz, P.; Komaromi, I.; Martin, R. L.; Fox, D. J.; Keith, T.; Al-Laham, M. A.; Peng, C. Y.; Nanayakkara, A.; Challacombe, M.; Gill, P. M. W.; Johnson, B.; Chen, W.; Wong, M. W.; Gonzalez, C.; Pople, J. A. *Gaussian 03*, revision B.05; Gaussian, Inc.: Pittsburgh, PA, 2004.

(22) (a) Willson, S. P.; Andrews, L. *J. Phys. Chem. A* **1999**, *103*, 3171. (b) Willson, S. P.; Andrews, L. *J. Phys. Chem. A* **1999**, *103*, 6972.

(23) Parker, D.; Dickins, R. S.; Puschmann, H.; Crossland, C.; Howard, J. A. K. *Chem. Rev.* **2002**, *102*, 1977.

(24) Martin, W. C.; Zalubas, R.; Hagan, L. Atomic Energy Levels - The Rare Earth Elements. *Natl. Stand. Ref. Data Series (U. S., Natl. Bur. Stand.)* **1978**, 60.

(25) Romas, K.; Ausra, K. *J. Phys. Chem. A* **1998**, *102*, 897.